

# Synthesis of CdSnO<sub>3</sub>·3H<sub>2</sub>O Nanocubes via Ion Exchange and Their Thermal Decompositions to Cadmium Stannate

Yiwen Tang,\* Yun Jiang, Zhiyong Jia, Bihui Li, Lijuan Luo, and Liang Xu

Institute of Nano-science and Technology, Central China Normal University, Wuhan 430079, China

Received July 22, 2006

Uniform crystalline CdSnO<sub>3</sub>·3H<sub>2</sub>O nanocubes with a 28–35 nm edge length have been obtained via the ion-exchange reaction of Na<sub>2</sub>Sn(OH)<sub>6</sub> in a CdSO<sub>4</sub> aqueous solution, assisted by ultrasonic treatment. Precursor Na<sub>2</sub>Sn(OH)<sub>6</sub> crystals were prepared via hydrothermal treatment in an ethanol/water solution. The formation of CdSnO<sub>3</sub>·3H<sub>2</sub>O nanocubes resulted from the strain during the ion-exchange process. The influences of reaction conditions, such as ion-exchange (ultrasonic treatment) duration, solvent constitutes, surfactant, and pH on the formation of CdSnO<sub>3</sub>·3H<sub>2</sub>O crystals were described. Crystalline CdSnO<sub>3</sub> and Cd<sub>2</sub>SnO<sub>4</sub> have been obtained by thermal treatment at 300 and 500 °C, respectively, for 5 h under an inert-gas protecting condition using CdSnO<sub>3</sub>·3H<sub>2</sub>O nanocubes as the precursor. The cube shape of CdSnO<sub>3</sub>·3H<sub>2</sub>O was sustained after thermal decomposition to CdSnO<sub>3</sub>.

## 1. Introduction

The synthesis of inorganic nanostructures with well-defined size, shape, composition, crystallinity, and structure, such as nanospheres, nanorods, nanowires, nanotubes, and nanocubes, has been an active research area because of the unique size- and shape-dependent properties<sup>1–5</sup> of these compounds, which are different from those of the bulk. These materials are important in the fields of catalysis, photography, electronics, photonics, data storage, optoelectronics, biological labeling, imaging, and biosensing.<sup>6–14</sup> Particular emphasis has recently been placed on the fine-tuning of the shape and size of inorganic materials, including the nanocube.<sup>15–24</sup>

Much remains to be investigated with regard to the controllable synthesis and property evaluation of these morphological novelties. For example, considerable strategies have been developed for growing cubes of metal oxides (Cu<sub>2</sub>O/Co<sub>3</sub>O<sub>4</sub>), halides (CaF<sub>2</sub>/BaF<sub>2</sub>), chalcogenides (Ag<sub>2</sub>S), etc.,<sup>15–21</sup> while comparatively little work has been performed on the ternary complex oxides (CaSnO<sub>3</sub>, Bi<sub>2</sub>Fe<sub>4</sub>O<sub>9</sub>).<sup>22–24</sup>

Among the perovskite-type alkaline earth stannates, cadmium stannate has been recently considered to be a new material for semiconductor gas sensors because of its high selectivity, sensitivity, and stability toward ethanol gas.<sup>24–27</sup> It is well-known that the gas-sensing mechanism belongs to

\* To whom correspondence should be addressed. Fax: +86 27 67861185. E-mail: ywtang@phy.cnu.edu.cn.

- (1) Alivisatos, A. P. *Science* **1996**, *271*, 933–937.
- (2) Cui, Y.; Lieber, C. M. *Science* **2001**, *291*, 851–853.
- (3) Sun, Y.; Xia, Y. *Science* **2002**, *298*, 2176–2179.
- (4) Sun, X. M.; Li, Y. D. *Chem.—Eur. J.* **2003**, *9*, 2229–2238.
- (5) Ahmadi, T. S.; Wang, Z. L.; Green, T. C.; Henglein, A.; El-Sayed, M. A. *Science* **1996**, *272*, 1924–1925.
- (6) Lewis, L. N. *Chem. Rev.* **1993**, *93*, 2693–2730.
- (7) Schön, G.; Simon, U. *Colloid Polym. Sci.* **1995**, *273*, 101–117.
- (8) Theys, R. D.; Sosnovsky, G. *Chem. Rev.* **1997**, *97*, 83–132.
- (9) Maier, S. A.; Brongersma, M. L.; Kik, P. G.; Meltzer, S.; Reuquicha, A. A. G.; Atwater, H. A. *Adv. Mater.* **2001**, *13*, 1501–1505.
- (10) Kamat, P. V. *J. Phys. Chem. B* **2002**, *106*, 7729–7744.
- (11) Pileni, M. P. *Adv. Funct. Mater.* **2001**, *11*, 323–336.
- (12) Malinsky, M. D.; Kelly, K. L.; Schatz, G. C.; van Duyne, R. P. *J. Am. Chem. Soc.* **2001**, *123*, 1471–1482.
- (13) Bruchez, M.; Moronne, M.; Gin, P.; Weiss, S.; Alivisatos, A. P. *Science* **1998**, *281*, 2013–2016.
- (14) Wang, J. F.; Gudiksen, M. S.; Cui, Y.; Lieber, C. M. *Science* **2001**, *293*, 1455–1457.

- (15) Lim, W. P.; Zhang, Z.; Low, H. Y.; Chin, W. S. *Angew. Chem., Int. Ed.* **2004**, *43*, 5685–5689.
- (16) Gou, L.; Murphy, C. J. *J. Mater. Chem.* **2004**, *14*, 735–738.
- (17) Xu, R.; Zeng, H. C. *Langmuir* **2004**, *20*, 9780–9790.
- (18) Li, X.; Gao, H.; Murphy, C. J.; Gou, L. *Nano Lett.* **2004**, *4*, 1903–1907.
- (19) Liu, F. K.; Ko, F. H. *Chem. Lett.* **2004**, *33*, 902–903.
- (20) Wang, Z.; Chen, X.; Liu, J.; Mo, M.; Yang, L.; Qian, Y. *Solid State Commun.* **2004**, *130*, 585–589.
- (21) Sun, X.; Li, Y. *Chem. Commun.* **2003**, *14*, 1768–1769.
- (22) Lu, Z. G.; Liu, J. F.; Tang, Y. G.; Li, Y. D. *Inorg. Chem. Comm.* **2004**, *7*, 731–733.
- (23) Park, T. J.; Papaefthymiou, G. C.; Moodenbaugh, A. R.; Mao, Y. B.; Wong, S. S. *J. Mater. Chem.* **2005**, *15*, 2099–2105.
- (24) Shannon, R. D.; Gillson, J. L.; Bouchard, R. J. *J. Phys. Chem. Solids* **1977**, *38*, 877–881.
- (25) Cardile, C. M.; Meinhold, R. H.; MacKenzie, K. J. *J. Phys. Chem. Solids* **1987**, *48*, 881–885.
- (26) Zhang, T. S.; Shen, Y. S.; Zhang, R. F. *Mater. Lett.* **1995**, *23*, 69–71.
- (27) Liu, Y. L.; Xing, Y.; Yang, H. F.; Liu, Z. M.; Yang, Y.; Shen, G. L.; Yu, R. Q. *Analy. Chem. Acta* **2004**, *527*, 21–26.

the surface-controlled type.<sup>28</sup> Nanocrystalline particles, exhibiting a large surface area, might be favorable for improving the sensitivity of gas-sensing material.<sup>29</sup> On the other hand, particles with different morphologies may show desirable features because these particles are nucleated and grown in epitaxial manner, exposing defined crystal planes.<sup>30</sup> Some research groups have reported that particles with different morphologies showed different sensitivity to gas, resulting from their different surface activity;<sup>31–32</sup> therefore, it is interesting to investigate the facial synthesis methodology of nanomaterials with special morphologies for their potential application in gas sensors. Cadmium stannate nanoparticles have been synthesized by the chemical coprecipitation method,<sup>26,27,33</sup> but no analogues with well-defined sizes and shapes (e.g., nanocubes) have been prepared. In the current work, we employed a two-step technique to synthesis uniform nanocrystallite  $\text{CdSnO}_3 \cdot 3\text{H}_2\text{O}$  cubes with a narrow particle size distribution. Our method involved the preparation of precursors  $\text{Na}_2\text{Sn}(\text{OH})_6$  via a hydrothermal method in an ethanol/water solution, followed by the ion-exchange reaction between solid  $\text{Na}_2\text{Sn}(\text{OH})_6$  crystals and  $\text{Cd}^{2+}$  solution, assisted by ultrasonic treatment. We have established that the ion-exchange (ultrasonic treatment) duration, surfactant, pH, and volume ratio of ethanol/water in the hydrothermal treatment process are crucial to the growth of  $\text{CdSnO}_3 \cdot 3\text{H}_2\text{O}$  nanocubes. Furthermore, crystalline  $\text{CdSnO}_3$  and  $\text{Cd}_2\text{SnO}_4$  have been obtained by thermal treatment at 300 and 500 °C, respectively, for 5 h under an inert-gas protecting condition using  $\text{CdSnO}_3 \cdot 3\text{H}_2\text{O}$  nanocubes as the precursor. The cube shape of  $\text{CdSnO}_3 \cdot 3\text{H}_2\text{O}$  was sustained after thermal decomposition to  $\text{CdSnO}_3$ .

## 2. Experimental Section

**2.1. Hydrothermal Process.** Stannic chloride ( $\text{SnCl}_4$ ), sodium hydroxide ( $\text{NaOH}$ ), cadmium sulfate ( $\text{CdSO}_4$ ), and polyvinylpyrrolidone (PVP,  $M_w \approx 30\,000$ ) were of analytical grade and used as supplied. In a typical procedure, 1.5 mmol of  $\text{SnCl}_4$  and  $2.5 \times 10^{-2}$  mmol of PVP (calculated by the repeated unit) were simultaneously dissolved in 50 mL of an ethanol/water (4/1 by v/v) solution. Ten milliliters of 12.5 mol/L  $\text{NaOH}$  aqueous solution was then added dropwise into the solution under vigorous stirring. The resulting slurry was transferred into a Teflon-lined stainless steel autoclave with a capacity of 100 mL, and it was sealed. The hydrothermal synthesis was performed under saturated water vapor pressure at 180 °C for 24 h, and then, the vessel was cooled to room temperature. The product,  $\text{Na}_2\text{Sn}(\text{OH})_6$ , was collected by centrifugation.

**2.2. Ion-Exchange Reaction.** Five millimoles of  $3\text{CdSO}_4 \cdot 8\text{H}_2\text{O}$  was dissolved in 300 mL of deionized water to obtain an aqueous solution. The precursor ( $\text{Na}_2\text{Sn}(\text{OH})_6$ ) obtained in the hydrothermal

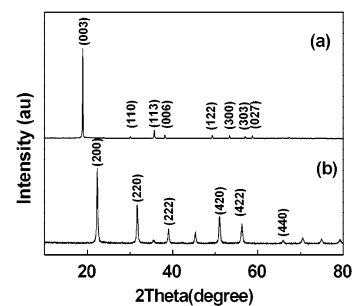


**Figure 1.** XRD patterns of the products (a)  $\text{Na}_2\text{Sn}(\text{OH})_6$  and (b)  $\text{CdSnO}_3 \cdot 3\text{H}_2\text{O}$ .

process was rapidly introduced to  $\text{CdSO}_4$  aqueous solution. The slurry was ultrasonically treated for 50 min, during which  $\text{Cd}^{2+}$  replaced the  $\text{Na}^+$  of  $\text{Na}_2\text{Sn}(\text{OH})_6$ . The resultant  $\text{CdSnO}_3 \cdot 3\text{H}_2\text{O}$  was filtered, washed with distilled water and ethanol, and then dried at room temperature.

**2.3. Thermal Treatment.** The as-prepared  $\text{CdSnO}_3 \cdot 3\text{H}_2\text{O}$  was subsequently calcined at 300 and 500 °C for 5 h under inert-gas protecting conditions (99.9% Ar).

**2.4. Material Characterization.** The crystallinity and phase purity of the product were examined by a Bruker D8 advance X-ray diffractometer (XRD) with monochromatized  $\text{Cu K}\alpha$  radiation ( $\lambda = 1.5418 \text{ \AA}$ ). The morphology and structure of the as-synthesized product were characterized using a JEOL JEM-2010 transmission electron microscope (TEM) operating at 200 kV and a JEOL JSM-6700F scanning electron microscope (SEM). The stoichiometry of the products was examined by X-ray photoelectron spectroscopy (XPS) using a Kratos XSAM 800 spectrometer with a  $\text{Mg K}\alpha$  (1253.6 eV) X-ray source. The X-ray gun was operated at 12 kV and 16 mA. The binding-energy scale was referenced to the main  $\text{C}_{1s}$  peak at 284.6 eV. Differential scanning calorimetric analysis (DSC) and thermogravimetric analysis (TGA) were carried out with a STA409PC LUX apparatus (Germany) with a heating rate of  $10 \text{ }^\circ\text{C min}^{-1}$  in a flowing  $\text{N}_2$  atmosphere. The particle size data were calculated by the line-intercept method using counting statistics for a group of 100 particles.

## 3. Results and Discussion

The XRD pattern (Figure 1a) of the sample prepared by hydrothermal treatment shows the formation of phase-pure  $\text{Na}_2\text{Sn}(\text{OH})_6$ , which matches well with the information for JCPDS file card 24-1143. The hexagonal lattice parameters obtained by least-squares fitting of the  $hkl$  and  $2\theta$  values are  $a = 5.94 \text{ \AA}$  and  $c = 14.1 \text{ \AA}$ . The much larger ratio between (003) and other low-intensity peaks in the XRD pattern in Figure 1a compared with that of standard JCPDS 24-1143 in the standard pattern database indicates that the preferred orientation of the  $\text{Na}_2\text{Sn}(\text{OH})_6$  is along the  $c$  axis. The SEM image in Figure 2a shows that  $\text{Na}_2\text{Sn}(\text{OH})_6$  has flat plates, which are assembled almost in parallel to form plate-stacks in different sizes. It is reasonable that the plates are crystals with preferred orientation as indicated by XRD.

$\text{CdSnO}_3 \cdot 3\text{H}_2\text{O}$  nanocubes were synthesized by the reaction between solid  $\text{Na}_2\text{Sn}(\text{OH})_6$  and the  $\text{CdSO}_4$  aqueous solution assisted by ultrasonic treatment. Figure 1b represents its XRD pattern. It is evident that all the reflections in Figure 1b can be readily indexed to the cubic phase ( $a = 8.00 \text{ \AA}$ ) of  $\text{CdSnO}_3 \cdot 3\text{H}_2\text{O}$  (JCPDS 28-0202). Figure 2b shows a representative SEM image of the as-prepared  $\text{CdSnO}_3 \cdot 3\text{H}_2\text{O}$ . It

(28) Tan, O. K.; Zhu, W.; Yan, Q.; Kong, L. B. *Sens. Actuators B* **2000**, *65*, 361–365.

(29) Huang, X. J.; Scoonman, J. *Sens. Actuators B* **1994**, *22*, 227.

(30) Xia, Y. N.; Yang, P. D.; Sun, Y. G.; Wu, Y. Y.; Marers, B.; Gates, B.; Yin, Y. D.; Kim, F.; Yan, H. Q. *Adv. Mater.* **2003**, *15*, 353–389.

(31) Zhou, K.; Wang, X.; Sun, X.; Peng, Q.; Li, Y. J. *Catal.* **2005**, *229*, 206–212.

(32) Chen, L. M.; Liu, Y. N.; Lu, Z. G.; Zeng, D. M. *J. Colloid Interface Sci.* **2006**, *295*, 440–444.

(33) Wu, X. H.; Wang, Y. D.; Liu, H. L.; Li, Y. F.; Zhou, Z. L. *Mater. Lett.* **2002**, *56*, 732–736.

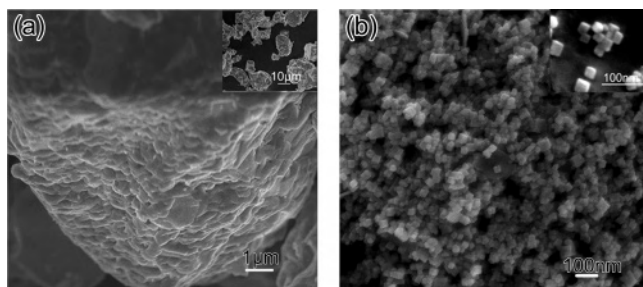


**Figure 2.** SEM images of the products (a)  $\text{Na}_2\text{Sn}(\text{OH})_6$  and (b)  $\text{CdSnO}_3 \cdot 3\text{H}_2\text{O}$ .

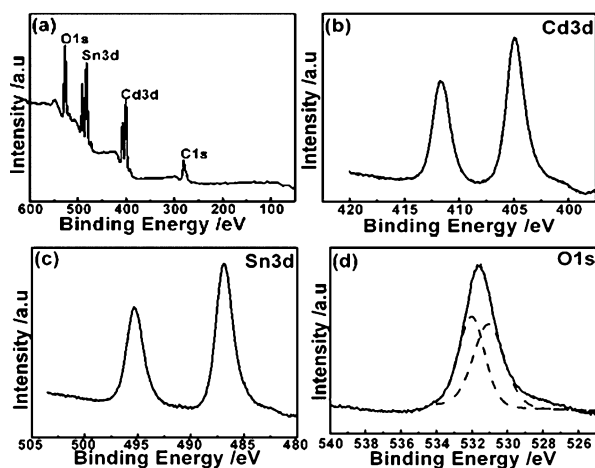


**Figure 3.** XPS spectra of the (a)  $\text{CdSnO}_3 \cdot 3\text{H}_2\text{O}$  nanocube and the (b)  $\text{Cd}_{(3d)}$ , (c)  $\text{Sn}_{(3d)}$ , and (d)  $\text{O}_{(1s)}$  regions.

can be clearly observed from the inset of Figure 2b that the  $\text{CdSnO}_3 \cdot 3\text{H}_2\text{O}$  product mainly consists of nanometer-scale cubes. The cubic edge length is in the range of 28–35 nm.

XPS analysis was performed to determine the stoichiometry of the product. The XPS spectrum for  $\text{CdSnO}_3 \cdot 3\text{H}_2\text{O}$  (Figure 3a) clearly shows  $\text{Cd}_{(3d)}$ ,  $\text{Sn}_{(3d)}$ ,  $\text{O}_{(1s)}$ , and  $\text{C}_{(1s)}$ . The absence of the Na peaks and  $\text{N}_{(1s)}$  indicated that the  $\text{Na}^+$  almost had been replaced by  $\text{Cd}^{2+}$  and that the PVP had been removed completely by washing. The other panels in Figure 3 show high-resolution XPS regions of various elements for the products. The peak locations of  $\text{Cd}_{(3d)}$  and  $\text{Sn}_{(3d)}$  are similar to the standard spectrum of  $\text{CdSnO}_3$ .<sup>34</sup> But the  $\text{O}_{(1s)}$  peak shifts toward higher binding energy with respect to the  $\text{CdSnO}_3$   $\text{O}_{(1s)}$  peak. The peaks could be fitted by two nearly Gaussian functions, centered at 530.4 and 532.4 eV, respectively. The low binding energy component located at ~530.4 eV is attributed to the  $\text{CdSnO}_3$  crystal lattice oxygen. The high binding component, centered at 532.4 eV, is associated with the presence of hydrated oxides species corresponding to  $\text{OH}$ .<sup>35</sup> The analysis of the  $\text{Cd}_{(3d)}$ ,  $\text{Sn}_{(3d)}$ , and  $\text{O}_{(1s)}$  peak intensities gives an atomic ratio of 1:1.07:6.04. The results reveal that the products are  $\text{CdSnO}_3 \cdot 3\text{H}_2\text{O}$  within the limits of instrumental error.

Herein, the two-step process plays an important role in the synthesis of  $\text{CdSnO}_3 \cdot 3\text{H}_2\text{O}$  nanocube. The preparation

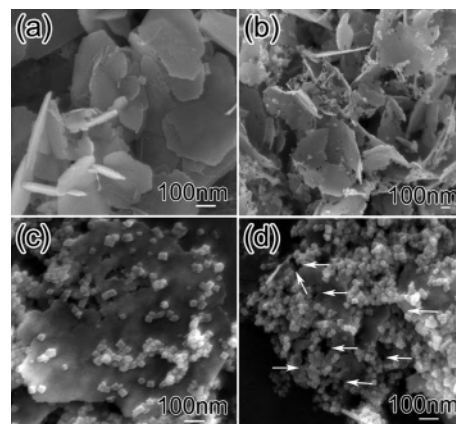


**Figure 4.** SEM images of the products prepared after different ion-exchange times: (a) 5, (b) 10, (c) 15, and (d) 20 min.

of  $\text{CdSnO}_3 \cdot 3\text{H}_2\text{O}$  is based on the following formal reactions



A hydrothermal reaction was carried out in an ethanol/water solution to obtain crystalline  $\text{Na}_2\text{Sn}(\text{OH})_6$ . The following reaction with the  $\text{CdSO}_4$  aqueous solution resulted in a white powdery product consisting of crystallites with cubic shapes that can be confirmed as  $\text{CdSnO}_3 \cdot 3\text{H}_2\text{O}$  by the XRD pattern (Figure 1b). The reaction is basically a diffusion-controlled ion-exchange process in which  $\text{Cd}^{2+}$  ions in the  $\text{CdSO}_4$  aqueous solution replace the  $\text{Na}^+$  ions of  $\text{Na}_2\text{Sn}(\text{OH})_6$  as the reaction proceeds, driven by, among other effects, the ion concentration gradient and entropy effect. To gain a better understanding of the nanocubes formation, we have studied the time course of the reaction by SEM. Figure 4 shows scenario images for the morphology evolution. When an  $\text{Na}_2\text{Sn}(\text{OH})_6$  crystal (Figure 2a) was placed into the  $\text{CdSO}_4$  aqueous solution, ion-exchange between  $\text{Cd}^{2+}$  and  $\text{Na}^+$  occurred via the surfaces of the  $\text{Na}_2\text{Sn}(\text{OH})_6$  particles in a relatively short time, which avoided the dissolution of  $\text{Na}_2\text{Sn}(\text{OH})_6$  in water. After 5 min of chemical reaction, the big  $\text{Na}_2\text{Sn}(\text{OH})_6$  particles split into many plates as shown in Figure 4a because the weak coupling between the original parallel plates was broken because of the coupling effects of reaction and sonication. Since the ionic radius of  $\text{Cd}^{2+}$  (95 pm) ion is smaller than that of  $\text{Na}^+$  (102 pm), as more and more ions are exchanged, the  $\text{Cd}_{0.5x}\text{Na}_{2-x}\text{Sn}(\text{OH})_6$  crystals became strained and unstable. When the strain exceeded a critical value, the  $\text{Na}_2\text{Sn}(\text{OH})_6$  structure then transformed into the more stable  $\text{CdSnO}_3 \cdot 3\text{H}_2\text{O}$  structure. The  $\text{CdSnO}_3 \cdot 3\text{H}_2\text{O}$  particles show cubic shapes mainly because their intrinsic structures have cubic symmetry. To release the strong stress and lower the total energy,  $\text{CdSnO}_3 \cdot 3\text{H}_2\text{O}$  nanocubes are detached from the plates. Figure 4b–d shows the SEM images taken from the product with 10, 15, and 20 min, respectively, of ion-exchange treatment. As the ion-exchange reaction continues, more and more nanocubes are produced. After 20 min treatment, one

(34) Golestani-Fard, F.; Hashemi, T.; Mackenzie, K. J. D.; Hogarth, C.A. *J. Mater. Sci.* **1983**, *18*, 3679–3685.

(35) Standard XPS data. <http://srdata.nist.gov/xps/>.

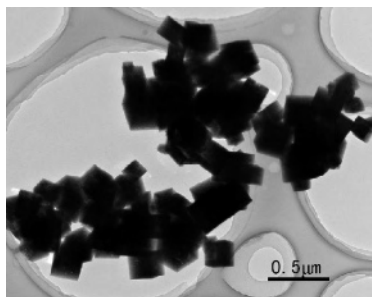


**Figure 5.** TEM image of the product with a 60 min ion-exchange treatment.

can see that the reaction is not complete, and many plates with holes are observed. It is also clear that the cubic hole or joint holes denoted by white arrows in the plates results from the separation of nanocubes. The ion-exchange reaction was complete at 50 min, using a typical procedure as shown in Figure 2b.

The two-step process plays a key role in obtaining uniform  $\text{CdSnO}_3 \cdot 3\text{H}_2\text{O}$  nanocubes. Control experiments were carried out to investigate the results of the one-step process. If the  $\text{SnCl}_4$ ,  $3\text{CdSO}_4 \cdot 8\text{H}_2\text{O}$ ,  $\text{NaOH}$ , and PVP solution is hydrothermally treated at  $180^\circ\text{C}$  for 24 h, the product not only consisted of larger cubic structures but also the distribution of sizes was wider. In addition, the pH has to be strictly adjusted to obtain cubic  $\text{CdSnO}_3 \cdot 3\text{H}_2\text{O}$ . Another experiment was performed in which purchased  $\text{Na}_2\text{SnO}_3 \cdot 3\text{H}_2\text{O}$  was put into  $3\text{CdSO}_4 \cdot 8\text{H}_2\text{O}$  aqueous solutions assisted by ultrasonic treatment. The product was dominated by microparticles with irregular shape. Thus, the formation of platelike  $\text{Na}_2\text{Sn}(\text{OH})_6$  crystal via hydrothermal treatment is a key process influencing the synthesis of uniform  $\text{CdSnO}_3 \cdot 3\text{H}_2\text{O}$  nanocubes.

In the experiments, the synthesis parameters, such as the ultrasonic treatment (ion-exchange) duration, solvent composition, surfactant, and pH, play an important role in the control of the size and composition of the final products. It is well-known that ultrasonic cavitation in liquid may improve the ion-diffusion rate and that it is effective for deagglomeration. Without ultrasonic treatment,  $\text{CdSnO}_3 \cdot 3\text{H}_2\text{O}$  cubes with a wide size distribution aggregate together and are difficult to deagglomerate after reaction. However, nanocubes with a uniform edge size of 30 nm can be obtained (Figure 2b) by ultrasonic treatment for 50 min. When the ultrasonic treatment time was increased to 60 min, the size of cubes increased from 30 (50 min) to 150 nm for only an additional 10 min of ultrasonic treatment (Figure 5). It can be proposed that, in the initial stage of ion-exchange reaction,  $\text{Cd}^{2+}$  and  $\text{Na}^+$  exchange rapidly and the  $\text{CdSnO}_3 \cdot 3\text{H}_2\text{O}$  nanocubes separate from the precursor plates assisted by ultrasound. With the time was increased, the turbulent flow and shock waves produce by acoustic cavitation can drive the nanocubes together and make them coalesce and grow. Thus, dispersed nanocubes with uniform edge size can be obtained under a suitable ultrasonic treatment (50 min). In addition, the ethanol environment is crucial to ensure the formation of  $\text{Na}_2\text{Sn}(\text{OH})_6$  crystals in an ethanol/water solution and the subsequent formation of  $\text{CdSnO}_3 \cdot 3\text{H}_2\text{O}$ . As shown by the XRD patterns in Figure 6, with a decrease of

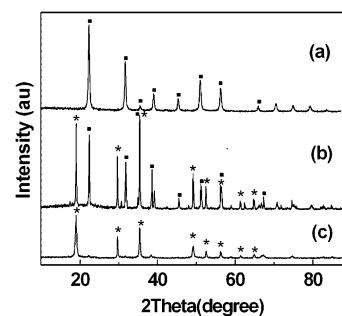


**Figure 6.** XRD patterns of composite prepared at different ratios of the ethanol/water solution: (a) 4:1, (b) 1:1, and (c) 1:4 [\*],  $\text{Cd}(\text{OH})_2$ ,  $\text{CdSnO}_3 \cdot 3\text{H}_2\text{O}$ ].

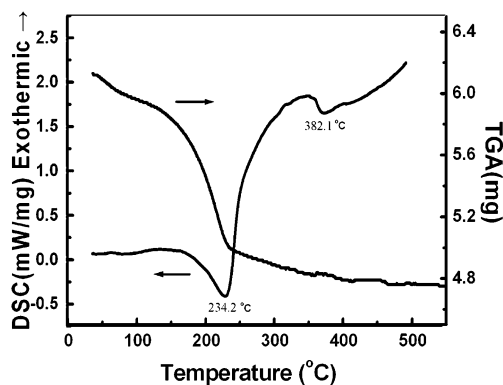


**Figure 7.** DSC and TGA curves of  $\text{CdSnO}_3 \cdot 3\text{H}_2\text{O}$ .

the volume ratio of the ethanol/water, the product shifts from  $\text{CdSnO}_3 \cdot 3\text{H}_2\text{O}$  and a mixture of  $\text{CdSnO}_3 \cdot 3\text{H}_2\text{O}/\text{Cd}(\text{OH})_2$  to  $\text{Cd}(\text{OH})_2$ . This is probably related to preferential formation of  $\text{Sn}(\text{OH})_4$  compared to that of  $\text{Na}_2\text{Sn}(\text{OH})_6$  with the increase of water resulting in a higher polarity in the hydrothermal system. The surfactant is always used to control the morphologies of nanostructures well.<sup>36–39</sup> Herein, to achieve the plate-shaped  $\text{Na}_2\text{Sn}(\text{OH})_6$  particles, we introduced PVP into the synthesis system. Although polyvinylpyrrolidone (PVP), poly(ethylene glycol) (PEG), and cetyl-trimethyl ammonium bromide (CTAB) have been used to control the shapes of nanomaterials, PVP was found to be unique in the present synthesis system. But the exact role of PVP in this process is unclear. Moreover, we also found that the  $\text{CdSnO}_3 \cdot 3\text{H}_2\text{O}$  nanocube could be obtained in any strong alkaline condition for this two-step method. It implies that the pH value has limited influence on the formation of  $\text{CdSnO}_3 \cdot 3\text{H}_2\text{O}$  nanocubes.

The thermal behavior of  $\text{CdSnO}_3 \cdot 3\text{H}_2\text{O}$  nanocubes was investigated with DSC and TGA measurements. As observed, the DSC curve in Figure 7 exhibits a weak endothermic peak at  $95^\circ\text{C}$ , and the TGA curve involves a continuous mass loss from room temperature to  $120^\circ\text{C}$ . These could be caused by the release of absorbed water. Two more endothermic

(36) Zhou, X. F.; Chen, S. Y.; Zhang, X. D.; Guo, X. F.; Ding, W. P.; Chen, Y. *Langmuir* **2006**, *22*, 1383–1387.

(37) Jana, N. R.; Gearheart, L.; Murphy, C. J. *Adv. Mater.* **2001**, *13*, 1389–1393.

(38) Li, C. C.; Cai, W. P.; Cao, B. Q.; Sun, F. Q.; Li, Y.; Kan, C. X.; Zhang, L. D. *Adv. Funct. Mater.* **2006**, *16*, 83–90.

(39) Yu, Y. T.; Xu, B. Q. *Appl. Organomet. Chem.* **2006**, *20*, 638–647.

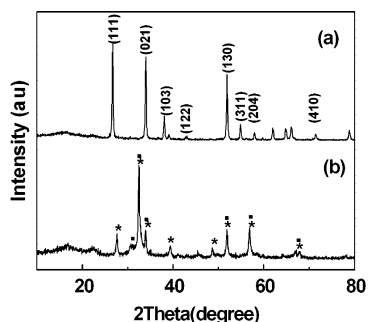


**Figure 8.** XRD patterns of the products (a)  $\text{CdSnO}_3$  and (b)  $\text{Cd}_2\text{SnO}_4$  (\*, cubic; ■, orthorhombic).

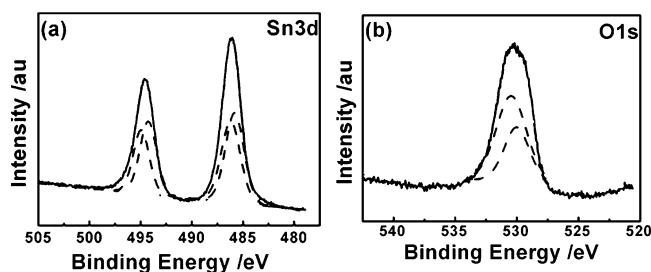
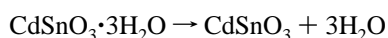


**Figure 9.** XPS spectra of the  $\text{Cd}_2\text{SnO}_4$ : (a)  $\text{Sn}_{(3d)}$  and (b)  $\text{O}_{(1s)}$  regions.

peaks with maxima located at 234 and 382 °C are also shown; these peaks are accompanied by weight losses of ~8.5 and ~0%, respectively. The first peak at 234 °C can be attributed to the loss of three water molecules according to



but its total mass loss is lower than the theoretical value (15.8%) calculated from the above equation. This suggests incomplete decomposition even around 234 °C. The second peak at 382 °C and its corresponding stable weight are attributed to the decomposition of the products according to

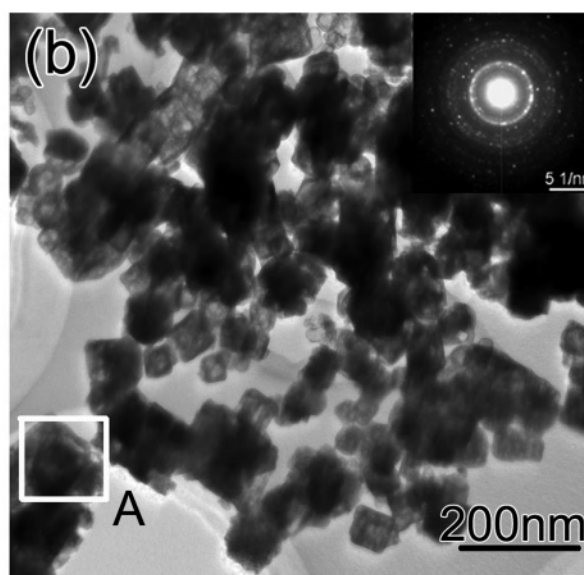
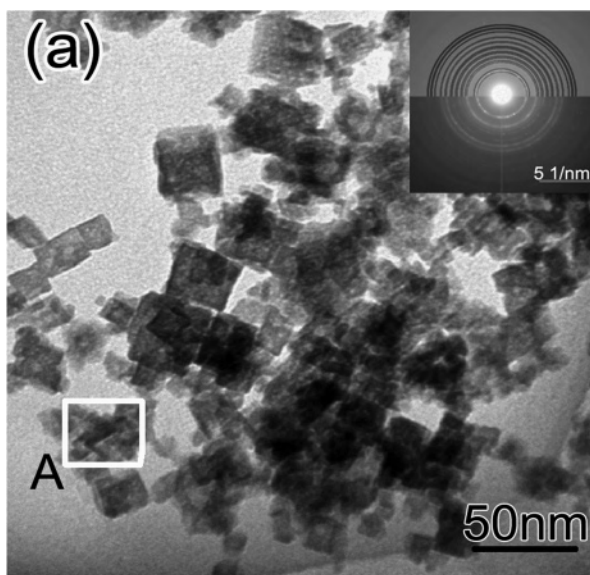


**Figure 10.** TEM and SAED images of the products (a)  $\text{CdSnO}_3$  and (b)  $\text{Cd}_2\text{SnO}_4$ .

On the basis of the thermal measurement results, we thermally treated  $\text{CdSnO}_3 \cdot 3\text{H}_2\text{O}$  at 300 and 500 °C for 5 h and investigated the phase of products by XRD measurement (Figure 8). All of the peaks in Figure 8a can be indexed to the orthorhombic  $\text{CdSnO}_3$  (JCPDS 34-0885) phase, indicating that  $\text{CdSnO}_3 \cdot 3\text{H}_2\text{O}$  crystals have been decomposed to  $\text{CdSnO}_3$  completely at 300 °C. The peaks in Figure 8b can be indexed to the mixture of orthorhombic (JCPDS 20-0188) and cubic  $\text{Cd}_2\text{SnO}_4$  (JCPDS 34-0928) phases. The presence of only the peaks of  $\text{Cd}_2\text{SnO}_4$  phase in Figure 8b suggests that  $\text{SnO}_2$  is possibly amorphous.

To demonstrate the presence of  $\text{SnO}_2$ , the XPS spectra are taken from the sample after it was annealed at 500 °C. As shown in Figure 9, the XPS spectra of  $\text{Sn}_{(3d)}$  and  $\text{O}_{(1s)}$  are fitted by multiple Gaussians. Compared with the  $\text{Sn}_{(3d)}$  binding energy of  $\text{Cd}_2\text{SnO}_4$ , the Sn binding energy shifts to higher energy, indicating that at least two Sn species are present in the sample. The peaks at 493.9 and 485.5 eV are from the  $\text{Cd}_2\text{SnO}_4$  crystal lattice Sn, while the peaks at 494.9 and 486.2 eV are from  $\text{SnO}_2$ . The  $\text{O}_{(1s)}$  spectrum consists of two branches, the strong one at 530.4 eV corresponding to  $\text{Cd}_2\text{SnO}_4$  and the small shoulder at 530.1 eV being assigned to  $\text{SnO}_2$ .<sup>40</sup>

The morphologies and microstructures of the final products  $\text{CdSnO}_3$  and  $\text{Cd}_2\text{SnO}_4$  were investigated with TEM and selected-area electron diffraction (SAED). As shown in Figure 10a, the cube shape was retained after heat treatment at 300 °C, but the size of nanocubes was reduced from an average of 30 nm to about 20 nm because of dehydration. The inset of Figure 10a is a SAED pattern (lower half, rings), taken from a randomly chosen area A of the as-prepared  $\text{CdSnO}_3$ . It exhibits rings with several spots indicating the crystal nature of the sample. A simulated SAED pattern of  $\text{CdSnO}_3$  crystal is shown in the upper half. A reasonable agreement between these two parts had been achieved. So the SAED pattern can be indexed as the reflections of the  $\text{CdSnO}_3$  structure, which is consistent with the result obtained from XRD. From Figure 9b, one can see the larger formless

product of Cd<sub>2</sub>SnO<sub>4</sub>. The SAED pattern in the inset of Figure 9b reveals that Cd<sub>2</sub>SnO<sub>4</sub> is crystalline in structure.

#### 4. Conclusions

A new and simple method based on a hydrothermal process and an ion-exchange reaction has been proposed to synthesize well-defined CdSnO<sub>3</sub>·3H<sub>2</sub>O nanocubes at high yields. It has been found that the formation of the Na<sub>2</sub>Sn(OH)<sub>6</sub> crystal was a key process and the ethanol/water volume ratio strongly affected the composition of product. The CdSnO<sub>3</sub>·3H<sub>2</sub>O nanocubes were formed because of the strain during the ion-exchange process. The duration of sonication also played a significant role in determining the

size of the CdSnO<sub>3</sub>·3H<sub>2</sub>O nanocubes. Crystalline CdSnO<sub>3</sub> and Cd<sub>2</sub>SnO<sub>4</sub> have been obtained by thermal treatment at 300 and 500 °C, respectively, for 5 h under an inert-gas protecting condition using CdSnO<sub>3</sub>·3H<sub>2</sub>O nanocubes as the precursor. The cube shape of CdSnO<sub>3</sub>·3H<sub>2</sub>O was sustained after thermal decomposition to CdSnO<sub>3</sub>.

**Acknowledgment.** This work was supported by the COSTIND and Ministry of Education of China under Grant A1420060185 and the Natural Science Foundation of Hubei Province (No. 2005ABA039) of China. The authors thank Professor Lizhi Zhang in Central China Normal University for his constructive suggestion.

---

(40) Setty, M. S.; Sinha, A. P. B. *Thin Solid Films* **1986**, *144*, 7–19.

IC0613715